Structure and Segmental Dynamics Relationship in Natural Rubber/Layered Silicate Nanocomposites during Uniaxial Deformation

ARTICLE *in* MACROMOLECULES · APRIL 2013

Impact Factor: 5.8 · DOI: 10.1021/ma4002353

Macromolecules

Article

pubs.acs.org/Macromolecules

Structure and Segmental Dynamics Relationship in Natural Rubber/Layered Silicate Nanocomposites during Uniaxial Deformation

Marianella Hernández,*[,†] Alejandro Sanz,[‡] Aurora Nogales,[‡] Tiberio A. Ezquerra,[‡] and Miguel A. López-Manchado*[,†]

[†]Instituto de Ciencia y Tecnología de Polímeros, ICTP-CSIC, Juan de la Cierva 3, Madrid 28006, Spain

[‡]Instituto de Estructura de la Materia, IEM-CSIC, Serrano 121, Madrid 28006, Spain

ABSTRACT: Synchrotron X-ray scattering and broad-band dielectric spectroscopy experiments were performed in order to analyze the effect of strain-induced orientation on the structure/segmental dynamics relationship in natural rubber/layered silicate nanocomposites. The presence of interfacial interaction between nanoparticle−polymer matrix is crucial in promoting strain-induced crystallization in NR nanocomposites, as evidenced by the correlation between structural magnitudes and dynamic parameters. In this sense, the addition of nanoclay leads to enhanced crystallinity and lower onset of crystallization, while the segmental relaxation slows down due to the restriction imposed by the anchoring of chain segments into the crystals, with evidence of an amorphous/semicrystalline transition around a strain ratio $\lambda = 2.5$.

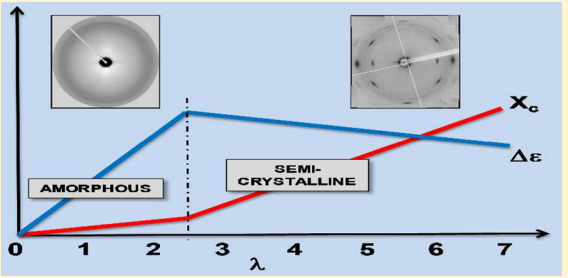

1. INTRODUCTION

Rubbers are polymeric materials endowed with the properties of flexibility and elastic extensibility. By the application of force, the molecules straighten out in the direction in which they are being pulled, and on release from being extended, they spontaneously recover their normal, random arrangements.

Rubbery behavior is exhibited by many polymeric materials. Among them natural rubber (NR) was the first to be industrially exploited. NR is nowadays complemented by a range of synthetic materials which have found niches in the market because of such characteristics as tensile strength, heat resistance, oil resistance, resistance to burning, and low air permeability. NR molecules consist mainly of *cis*-1,4-polyisoprene with practically no evidence for any *trans* materials, in contrast to the synthetic polyisoprenes.[1] The very flexible backbone leads to a very low glass transition temperature (T_g) of about −64 °C. Besides, due to its highly regular structure, NR is capable of crystallizing.[2] Crystallization may also be induced by stretching samples such as in a tensile test. As a result of this strain-induced crystallization, the tiny crystal structures formed act like reinforcing particles and enable NR to exhibit high strength. When the rubber is stretched, the internal shearing action tends to align the long molecules preferentially in the stretching direction, and this orientation can be detected by optical methods.

Moreover, the phenomenon of strain-induced crystallization (SIC) in NR composites has recently attracted much attention due to the fast development of nanocomposites. Rault et al.,[3,4] Poompradub et al.,[5] and Ozbas et al.,[6] for example, investigated the SIC of NR filled with carbon black and with functionalized graphene sheets using techniques such as ^{2}H NMR and synchrotron wide X-ray diffraction (WAXD) measurements. It was shown that the micromorphology of the filled NR network changed by stretching, resulting in earlier onset and stronger ability of crystallization. The effect of two-dimensional plate-shaped nanoclay with high aspect ratios on NR microstructure when stretched was also studied by Carretero et al.[7,8] and by Huang et al.[9,10] More recently, the reinforcement mechanism of NR composites with nanoalumina,[11] carbon nanofibers,[12] MWCNT,[13] and with functionalized graphene sheets[14,15] has attracted the attention of the scientific community. Despite all the extensive studies on this subject, there is still a lack of information on the relationship between mechanical strain and chain dynamics. Thus, in an attempt to better understand the effect of strain-induced orientation on the segmental dynamics of vulcanized NR/layered silicate nanocomposites, a series of synchrotron X-ray scattering and broad-band dielectric spectroscopy (BDS) experiments have been performed and are discussed in the following paragraphs, as a complementary study of previous work done by the authors on stretched vulcanized NR.[16]

2. EXPERIMENTAL SECTION

2.1. Materials. Natural rubber (NR) was kindly supplied by Malaysian Rubber (Berhad, Malaysia) under the trade name SMR CV60 (Mooney viscosity: ML(1 + 4) 100 °C = 60). A commercial montmorillonite organically modified named Cloisite15A (C15A) provided by Southern Clay Products Inc. (Gonzales, TX) was employed. The compounding ingredients were all commercial grades and were added to the rubber. The formulation and ingredients used to prepare vulcanized NR nanocomposites are compiled in Table 1.

Received: February 1, 2013
Revised: April 2, 2013
Published: April 12, 2013

Table 1. Formulation and Ingredients Used in the Preparation of Vulcanized NR/C15A Nanocomposites

ingredient	parts per hundred parts of rubber (phr)
NR	100.0
zinc oxide	5.0
stearic acid	1.0
MBTS[a]	1.0
sulfur	2.5
C15A	0.0[b]−5.0

[a]Mercaptobenzothiazyl disulfide. [b]Formulation corresponding to unfilled NR.

2.2. Sample Preparation. All ingredients were mixed in an open two-roll laboratory mill at room temperature. The rotors operated at a speed ratio of 1:1.4. Rubber nanocomposites were vulcanized in an electrically heated hydraulic press. NR films, 0.25 mm thick, were cured at 150 °C for 15 min according to the optimum cure time (t_{90}) derived from the curing curves previously determined by means of a Rubber Process Analyzer (RPA2000 Alpha Technologies). Rectangular-shaped specimens were mechanically cut out from the vulcanized film samples.

2.3. Experimental Methods. In order to study the strain-induced crystallization behavior in NR/layered silicate nanocomposites, samples with strain ratios (λ) from 1 to 7 were prepared. The strain ratio is defined as $\lambda = l/l_0$, in which l_0 is the initial length of the sample and l is the length of the elongated one. Tensile stress−strain properties of NR nanocomposites were measured at a cross-head speed of 500 mm/min following the procedure described by the authors elsewhere.[16]

Broad-band dielectric spectroscopy (BDS) measurements were performed on an ALPHA high-resolution dielectric analyzer (Novocontrol Technologies GmbH, Hundsangen, Germany). The stretched sample−electrode assembly was mounted in the dielectric cell between two parallel gold-plated electrodes. The complex permittivity ε^* of a given sample was calculated from the measurement of the complex impedance.[17] The complex permittivity of the stretched samples was measured over a frequency window of $10^{-1} < F/\mathrm{Hz} < 10^7$ ($F = \omega/2\pi$ is the frequency of the applied electric field being ω the angular frequency) in the temperature range from −100 to 100 °C in 5 °C steps. The imaginary part ε'' of the obtained dielectric permittivity, referred to as dielectric loss,[18,19] was analyzed by the phenomenological Havriliak−Negami (HN) function

$$\varepsilon^*(\omega) = \varepsilon_\infty + \frac{\varepsilon_s - \varepsilon_\infty}{[1 + (i\omega\tau_{HN})^b]^c} \quad (1)$$

where $\Delta\varepsilon = \varepsilon_s - \varepsilon_\infty$, ε_∞ and ε_s are the unrelaxed and relaxed values of the dielectric constant, and b and c are shape parameters ($0 < b, c \leq 1$) which describe the symmetric and the asymmetric broadening of the equivalent relaxation time distribution function, respectively. τ_{HN} is the Havriliak−Negami relaxation time, representing the most probable relaxation time of the relaxation time distribution function.[20] τ_{HN} is related to the frequency of maximum loss, $F_{max} = 1/(2\tau\pi_{max})$, by the equation[19,21]

$$\tau_{max} = \frac{1}{2\pi F_{max}} = \tau_{HN}\left[\sin\frac{b\pi}{2+2c}\right]^{-1/b}\left[\sin\frac{bc\pi}{2+2c}\right]^{1/b} \quad (2)$$

Both characteristic relaxation times coincide when the relaxation spectrum is symmetric, $c = 1$.

Wide-angle (WAXS) and small-angle (SAXS) X-ray scattering measurements of the stretched samples were carried out at the BM16 beamline[22] in the European Synchrotron Radiation Facility (ESRF) in Grenoble, France. Each stretched sample-frame assembly was placed in the beam path. The wavelength of the X-rays used was 0.9795 Å. The two-dimensional WAXS patterns were recorded using a MarCCD camera (X-ray Research, GmbH, Norderstedt, Germany). The image acquisition time for each frame was 3 s for WAXS and 1 s for SAXS. The diffraction angle was calibrated by a standard sample of alumina. All measured images were corrected for background, beam fluctuations, and sample absorption. The data analysis software FIT2D was used to analyze the WAXS/SAXS images.

3. RESULTS AND DISCUSSION

3.1. Stress−Strain Behavior and Development of Crystallites. It has been recognized that the excellent tensile properties of NR originate from its strain-induced crystallization upon elongation. Since striking improvements in the mechanical properties can be achieved at low loadings of nanoclay, one wonders if these improvements result from an increase in the crystallized fraction. Thus, the evolution of the crystallization behavior of the NR/C15A nanocomposites during stretching was determined. Figure 1 shows the stress−strain curve and corresponding WAXS/SAXS patterns at selected strain ratios for the NR filled with 5 phr of nanoclay C15A. The corresponding stress−strain curve for the unfilled NR is included for comparison.[16] The upturn of stress for the nanocomposite shifts to lower values of strain when compared to that of the vulcanized NR. Incipient contribution of crystalline reflections seem to appear already at a strain ratio λ = 2.5. The clear presence of these reflections at λ = 3.0 indicates that the nanocomposite has a smaller onset strain (λ^0) of crystallization than that of the matrix. Besides, all patterns exhibit preferred orientation of NR chains, which is evidenced by the alignment of the (200) and (120) reflections of the crystalline phase of the rubber matrix. As expected the intensities of the reflections increase with strain during stretching, while no preferred orientation of the amorphous phase is observed. A significant amount of amorphous phase is not oriented even under high strains, and a substantial amount of amorphous chains remains in a random coil conformation at high extension. Under deformation, the WAXS patterns show the superposition of an oriented crystal diffraction pattern and a residual amorphous halo. This strong isotropic amorphous halo

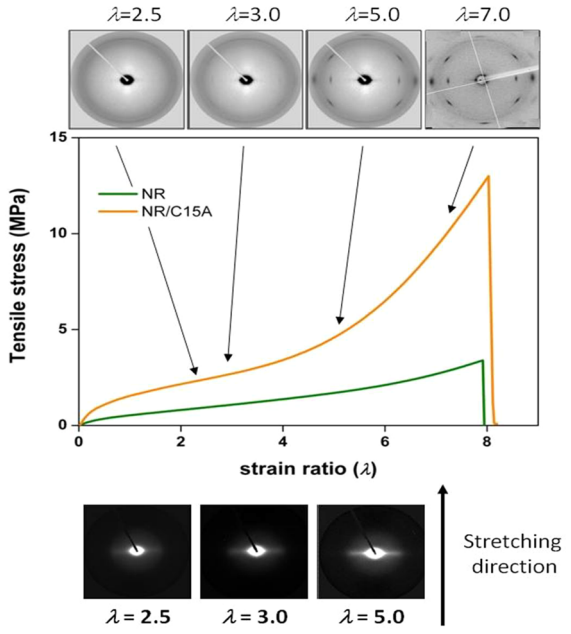

Figure 1. Representative stress−strain curves of NR and NR/C15A nanocomposite with corresponding synchrotron WAXS/SAXS (top/bottom) patterns during uniaxial deformation for NR/C15A nanocomposite.

dx.doi.org/10.1021/ma4002353 | Macromolecules 2013, 46, 3176−3182

persists, even at high strain ratios ($\lambda > 5$). This behavior is in accordance with results published by Toki et al.,[23−25] by Tosaka et al.,[26] and by Valladares et al.[27]

The procedure followed for the estimation of the crystallinity index was based on the equator diffraction peaks, as previously detailed in recent work for NR samples.[16] The diffraction intensity near the equator was normalized and azimuthally integrated in a cake from 75° to 105°, as shown in Figure 2. It is also noteworthy that the overall crystallinity index values in NR/C15A nanocomposites are higher than those for the pure rubber (see Figure 3). Thus, it is evidenced that the nature of the layered silicate particles plays a key role on the emerging of the first crystallites as well as on the final crystalline content during the deformation of the NR.

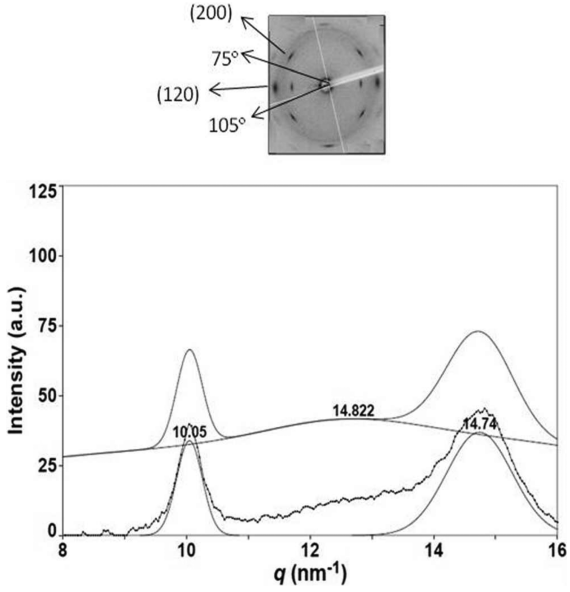

Figure 2. Equatorial cake integrated intensity as a function of the scattering vector q taken from the WAXS pattern of stretched NR/C15A nanocomposite at $\lambda = 7.0$. Inset shows integration limits from 75° to 105°.

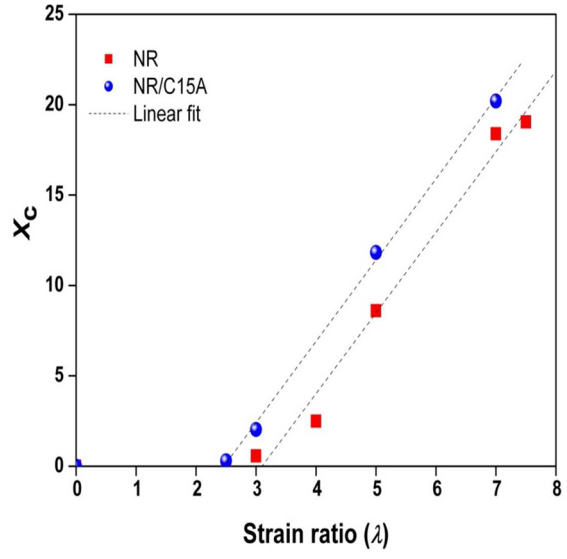

Figure 3. Crystallinity index X_c as a function of strain ratio λ for NR and NR/C15A nanocomposite. Dotted lines correspond to a linear fit.

The onset of crystallization was calculated by interception of the regression line in the plot of crystallinity index against strain ratio,[5,11] obtaining a strain ratio value of $\lambda^0 = 2.46$ for the nanocomposite and a value of $\lambda^0 = 3.09$ for the unfilled rubber (see Figure 3). The lower λ^0 of the nanocomposite reveals that an earlier orientation of rubber chains occurs. Upon deformation, exfoliated silicate layers existing within the NR matrix can align along the stretching direction at a very low strain ratio. Because of the attractive interaction between polymer chains and the nanoclay, the alignment of the nanoclay triggers the early orientation of more polymer chains. Furthermore, on the basis of the mechanism proposed by Tosaka et al.,[26,28] strain-induced crystals nucleate from the stretched network chains. Thus, the fact that more polymer chains can be stretched indicates that more nuclei can be formed.[9]

SAXS provides microstructure information about the distribution of clay particles in the NR matrix. The presence of streaks on the equator is clearly recognized in the SAXS patterns displayed in Figure 1 (bottom). The highly anisotropic SAXS peaks confirm the orientational alignment of exfoliated silicate layers in the NR matrix along the stretching direction.

3.2. Strain-Induced Changes in the Dynamics of Natural Rubber/Layered Silicate Nanocomposites. Natural rubber is primarily composed of *cis*-1,4-polyisoprene (PI) chains. Because of the lack of symmetry in the chemical structure of *cis*-PI, the polymer has components of the dipole moment both parallel and perpendicular to the chain contour. Therefore, *cis*-PI exhibits a dielectric normal-mode process caused by the parallel dipole moment as well as a segmental-mode process, which has its origin in local motions of the perpendicular dipole moment.[17,29]

At this point, it is important to highlight that our research is based on NR. Even though this material has the same chemical structure of synthetic *cis*-PI, NR contains significant amounts of proteins and lipids that are not present in the synthetic peer. These components induce a multiscaled microstructure characterized by a naturally occurring network with different dynamic response.[30] Moreover, in this investigation we are dealing with vulcanized NR samples; therefore, the normal mode process vanishes due to the cross-linking and the concurrent loss of significant dynamics.[31]

Segmental Mode. Figure 4 shows the dielectric loss curves for the segmental mode as a function of frequency at different strain ratios. In the temperature range studied, the segmental relaxation moves slightly to lower frequencies, broadens, and exhibits weaker loss intensity at high strain ratios.

The dielectric spectra were fitted to the HN function. The characteristic parameters of this function such as $\Delta\varepsilon$, b, c, and τ_{HN} were obtained. Figure 5 shows the dependence of these parameters with the strain ratio. The behavior of the crystallinity index with strain ratio has also been included in this figure in order to visualize the global effect and to correlate structural magnitudes with dynamic parameters extracted from the dielectric measurements, even though measurements were done at different temperatures. The main driving force to analyze simultaneously structural and dynamic experiments is to have access to information relating both the crystalline and the amorphous phases. In a first approach, the dielectric strength is related to the amount of mobile amorphous phase

dx.doi.org/10.1021/ma4002353 | Macromolecules 2013, 46, 3176−3182

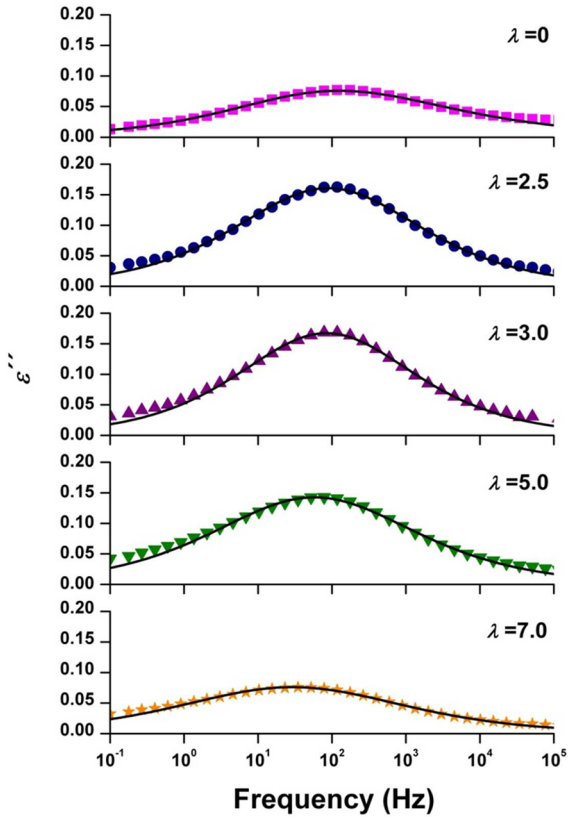

Figure 4. Frequency dependence of dielectric loss ε'' of NR/C15A nanocomposite samples stretched at different strain ratios as indicated on the plot in the region of the segmental mode (T = −40 °C). Solid lines correspond to the best HN fitting.

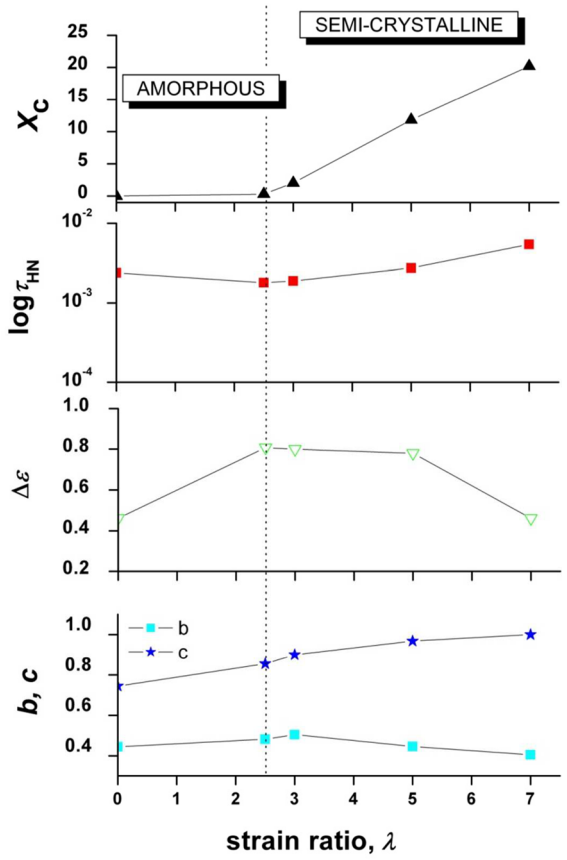

Figure 5. From top to bottom: (a) crystallinity index X_c at room temperature, (b) segmental relaxation time τ_{HN}, (c) dielectric strength $\Delta\varepsilon$, and (d) dielectric shape parameters (b, c), as a function of strain ratio for the vulcanized NR/C15A nanocomposite samples. The dielectric magnitudes have been extracted from measurements done at T = −40 °C.

while crystallinity relates to the amount of material included in the crystals.

Dielectric parameters were extracted from measurements at T = −40 °C, while the crystallinity index was measured at room temperature. To our knowledge, the crystalline structure is not expected to change upon cooling because the temperature scan at which BDS was performed was not slow enough for crystallization to take place. Moreover, Toki et al.[24] have reported similar behavior in an in-situ synchrotron X-ray diffraction study of three kinds of vulcanized polyisoprene rubber samples during uniaxial deformation at 0 °C. Also, Gent[32] has reported that the rate of crystallization of raw NR decreases continuously on lowering the temperature further than −26 °C, being the half-life time of crystallization at −26 °C around 10^2 min. A similar temperature dependence is also found for vulcanized NR, with a crystallization rate even lower.

The dependence of the dielectric magnitudes of the NR/C15A nanocomposite can be separated into two regimes, in a similar way to NR.[16] In a first approximation, the transition between the two regimes seems to be located at a strain ratio λ = 2.5. The trends in almost all the parameters are in accordance with the ones previously discussed for NR (τ_{HN} increases, b decreases, and c approaches unity with the strain ratio). The relaxation time, τ_{HN}, tends to increase slightly with the strain once crystallization appears. This effect can be expected since a reduced segmental mobility of the amorphous regions is imposed by the presence of the crystals, and more cooperativity is needed in order to accomplish segmental motions. In the crystallization region, the exponent b decreases and c increases. This indicates that the distribution of relaxation times becomes broader with the development of crystallinity. This effect has been generally observed during crystallization of polymer materials[33,34] and can be understood considering the model proposed by Schönhals and Schlosser, suggesting that the b parameter is related to large-scale motions and the $b \times c$ product to the small-scale motions of the segmental dymamics.[35] This model allows one to interpret the observed broadening and symmetrization of the α-relaxation in polymers during crystallization as due to restriction in the long-scale motions of the polymeric chains as the material is filled in with crystals. However, the observed decrease in b due to crystallization upon stretching in our case is significantly smaller than that generally observed in linear polymers. It is known that the deformation mechanism of the rubber network produces a characteristic nanostructure different for that typically observed for linear semicrystalline polymers. For vulcanized NR, a highly heterogeneous distribution of small crystallites embedded in an amorphous phase rich in random coil chains has been proposed.[26] Thus, in vulcanized NR and in the vulcanized NR nanocomposites, the restriction imposed to the segmental relaxation by crystals seems to be less effective than that observed in linear polymers for comparable values of crystallinity as a result of the different nanostructure.

With regard to the behavior of $\Delta\varepsilon$, at the initial stages of crystallization (low values of X_c) it is expected an increase of the density by stretching and a possible increase of the effective

dx.doi.org/10.1021/ma4002353 | Macromolecules 2013, 46, 3176−3182

dipole moment μ_{eff}^2 upon stretching, which support the increment in $\Delta\varepsilon$.[16] As crystallization proceeds, $\Delta\varepsilon$ decreases with the crystallinity index due to the decrease in the total number of dipole groups that relax through the α-process as more crystalline domains are formed, since more chain segments in the crystalline−amorphous interphase become a part of the crystalline regions.[36,37] The observed tendency on $\Delta\varepsilon$ does not change with temperature, as seen in Figure 6.

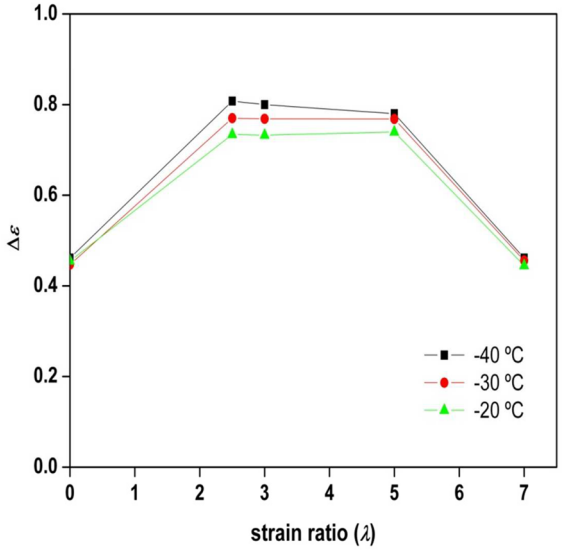

Figure 6. Dielectric strength as a function of strain ratio at different temperatures, as indicated in the plot.

Segmental relaxation times, τ_{max}, are plotted against the reciprocal temperature in Figure 7.

The relaxation times are well described over the measured range by the Vogel−Fülcher−Tamman (VFT) function $\tau = \tau_0 \exp(B/(T - T_0))$.[16] The parameters obtained from the best fit

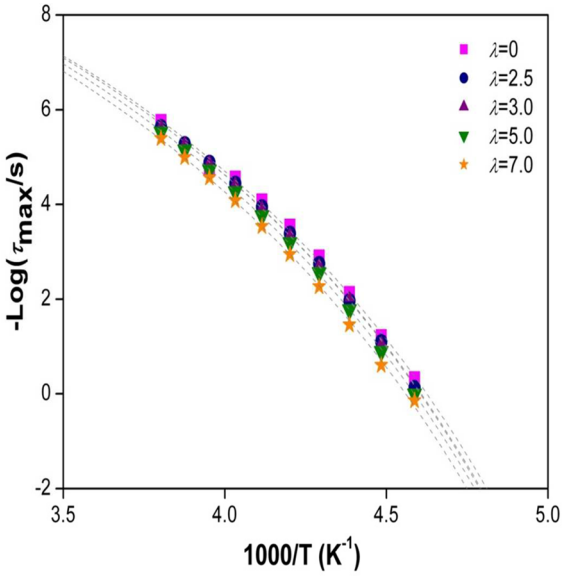

Figure 7. Activation plot of the average relaxation time for the segmental mode of NR/C15A nanocomposite stretched samples as a function of strain ratio. The dotted lines represent the fits to the VFT equation.

are summarized in Table 2, where one can see that the strain ratio has little effect on T_0. To reduce the effect of data fitting

Table 2. VFT Parameters for the Segmental Mode Process of NR/C15A Nanocomposite Samples Stretched at Different Strain Ratios

strain ratio (λ)	T_0 (K)	B (K)
0	149.4	935.6
2.5	160.5	833.3
3.0	160.1	856.7
5.0	159.7	876.6
7.0	159.2	892.1

to the VFT equation over a limited frequency range, a value of $\log \tau_0 \approx -14$ s was assumed according to previous work.[38] This assumption does not affect the quality of the data fit into the VFT equation but reduces the dispersion among fitting parameters.

New Mode. According to previous work reported by the authors,[31] the dielectric spectrum of the NR/C15A nanocomposites presents a relaxation process at high temperatures known as new mode, attributed to the segmental dynamics of polymer chains at the interfacial polymer−filler regions. Thus, the dielectric loss measurements of the NR/C15A nanocomposites stretched at different strain ratios were also performed as a function of frequency in the region of the new mode. Figure 8 shows the evolution of the dielectric loss as a function of frequency at T = 40 °C. This relaxation is

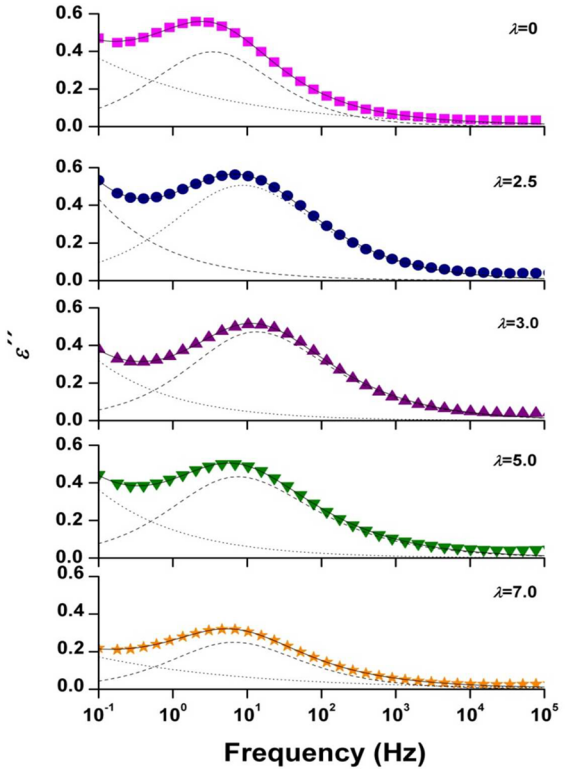

Figure 8. Frequency dependence of dielectric loss ε'' of NR/C15A nanocomposite samples stretched at different strain ratios as indicated on the plot in the region of the new mode (T = 40 °C). Solid lines correspond to best HN fitting, dashed lines to the individual process, and dotted lines to the conductivity contribution.

dx.doi.org/10.1021/ma4002353 | Macromolecules 2013, 46, 3176−3182

manifested by a clearly resolved maximum which exhibits weaker loss intensity at high strain ratios.

With regard to the temperature dependence of the new mode, the data shown in Figure 9 reveal that this relaxation does not present the curvature characteristic of a Vogel–Fülcher–Tamman (VFT) behavior, having an almost Arrhenius dependence.

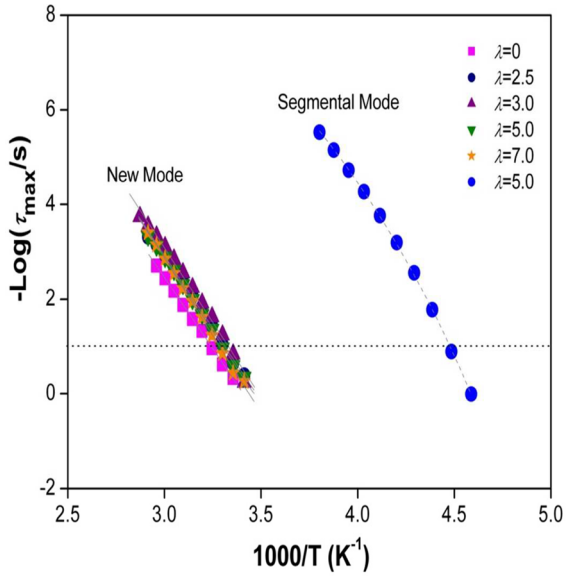

Figure 9. Activation plot of the average relaxation time for the new mode of NR/C15A nanocomposite stretched samples, as a function of strain ratio. The curve corresponding to the segmental mode of the NR/C15A nanocomposite at $\lambda = 5$ has been include for comparative purposes.

In order to further analyze the dependency of this new relaxation with the strain ratio, Figure 10a illustrates the temperature at which the average relaxation time of the new mode reaches a value of 0.1 s. It becomes evident that this dependence can be well separated into two regimes. In the first regime, for $\lambda < 2.5$, a clear decrease in temperature is observable, indicating a fastening of this relaxation upon stretching. As mentioned above, since the new mode of NR/C15A is related to a restricted NR phase associated with the clay interface then, the observed increment in mobility can be associated with the detachment of the restricted NR phase from the clay surface and therefore to a decrease in the NR–clay interaction. Further extension ($\lambda > 2.5$) provokes an increment in the reference temperature, indicating that the motion capability of the chain segments is reduced. Since in this stretching region crystallization is operative, it is straightforward to associate this effect to the restriction imposed by the anchoring of segment chains into the crystals.

Figure 10 also shows the dependence of $\Delta\varepsilon$ and τ_{HN} with the strain ratio for the segmental and new mode of the NR/C15A nanocomposite. Data corresponding to the segmental mode of NR have been included for comparative purposes. On the basis of these results, it becomes evident that the amorphous to semicrystalline transition on the segmental dynamics of the stretched NR/C15A nanocomposite samples is also present in the new mode. This transition leads to important changes on the segmental and new mode dynamics of the nanocomposites: (1) an important decrease of the dielectric strength and (2) a slowing down of both relaxations. These effects further support the similar segmental nature of both relaxations.

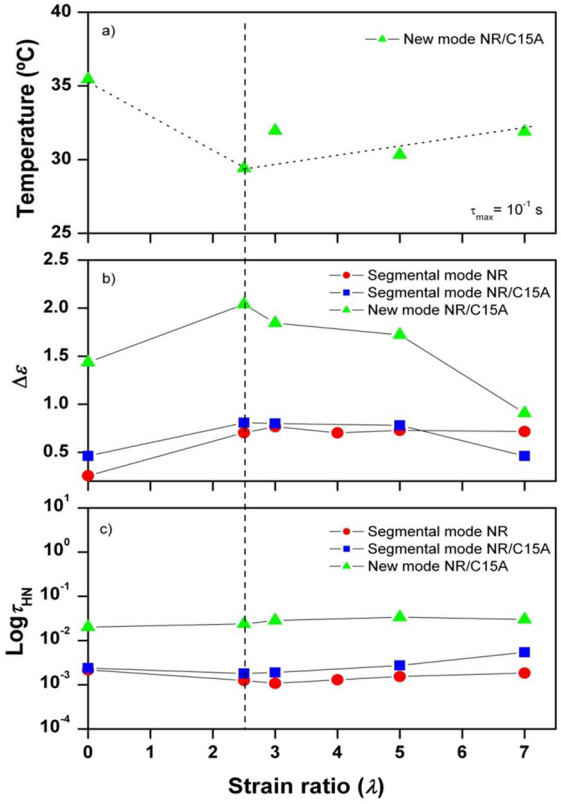

Figure 10. (a) Temperature and (b, c) dielectric parameters dependence with the strain ratio for the segmental and new mode of NR and NR/C15A nanocomposites. Dotted lines are guides for the eye.

4. CONCLUDING REMARKS

The effects of strain-induced crystallization on the molecular dynamics of vulcanized NR/layered silicate nanocomposites have been studied by means of broad-band dielectric spectroscopy and X-ray scattering techniques. Addition of nanoclay leads to enhanced crystallinity and lower onset strain for stretch-induced crystallization compared to unfilled NR. The dynamics of the NR nanocomposites is clearly affected by uniaxial stretching with a slowing down of the segmental relaxation, a decrease of the dielectric strength, and a broadening of the relaxation process. Besides, the new mode present in NR/layered silicate nanocomposites is also affected by the strain-induced crystallization phenomenon, with evidence of an amorphous/semicrystalline transition around $\lambda = 2.5$. The presence of interfacial interaction between nanoparticle–polymer matrix is crucial in promoting strain-induced crystallization in NR nanocomposites, as evidenced by the correlation between structural magnitudes with dynamic parameters.

AUTHOR INFORMATION

Corresponding Author

*E-mail: marherna@ictp.csic.es (M.H.); lmanchado@ictp.csic.es (M.A.L.-M.).

Notes

The authors declare no competing financial interest.

dx.doi.org/10.1021/ma4002353 | Macromolecules 2013, 46, 3176–3182

■ ACKNOWLEDGMENTS

This work was partially supported by MICINN Grants MAT2008-03232, MAT2010-18749, MAT2011-23455, and MAT2012-33517. M. Hernández gratefully acknowledges the Mision Ciencia fellowship from the Venezuelan Ministry of Science and Technology.

■ REFERENCES

(1) Brydson, J. A. *Rubbery Materials and Their Compounds*; Elsevier Science Publishers Ltd.: Essex, 1988; p 469.
(2) Brydson, J. A. *Plastics Materials*, 4th ed.; Butterworths: London, 1982; p 800.
(3) Trabelsi, S.; Albouy, P. A.; Rault, J. *Macromolecules* **2003**, *36* (24), 9093−9099.
(4) Rault, J.; Marchal, J.; Judeinstein, P.; Albouy, P. A. *Macromolecules* **2006**, *39* (24), 8356−8368.
(5) Poompradub, S.; Tosaka, M.; Kohjiya, S.; Ikeda, Y.; Toki, S.; Sics, I.; Hsiao, B. S. *J. Appl. Phys.* **2005**, *97* (10), 103529.
(6) Ozbas, B.; Toki, S.; Hsiao, B. S.; Chu, B.; Register, R. A.; Aksay, I. A.; Prud'homme, R. K.; Adamson, D. H. *J. Polym. Sci., Part B: Polym. Phys.* **2012**, *50* (10), 718−723.
(7) Carretero-Gonzalez, J.; Verdejo, R.; Toki, S.; Hsiao, B. S.; Giannelis, E. P.; López-Manchado, M. A. *Macromolecules* **2008**, *41* (7), 2295−2298.
(8) Carretero-González, J.; Retsos, H.; Verdejo, R.; Toki, S.; Hsiao, B. S.; Giannelis, E. P.; López-Manchado, M. A. *Macromolecules* **2008**, *41* (18), 6763−6772.
(9) Qu, L.; Huang, G.; Liu, Z.; Zhang, P.; Weng, G.; Nie, Y. *Acta Mater.* **2009**, *57* (17), 5053−5060.
(10) Nie, Y. J.; Huang, G. S.; Qu, L. L.; Wang, X. A.; Weng, G. S.; Wu, J. R. *Polymer* **2011**, *52* (14), 3234−3242.
(11) Nie, Y.; Huang, G.; Qu, L.; Zhang, P.; Weng, G.; Wu, J. *Polym. Adv. Technol.* **2011**, *22* (12), 2001−2008.
(12) Jiang, H.-X.; Ni, Q.-Q.; Natsuki, T. *Polym. Compos.* **2010**, *31* (6), 1099−1104.
(13) Weng, G. S.; Huang, G. S.; Qu, L. L.; Nie, Y. J.; Wu, J. R. *J. Phys. Chem. B* **2010**, *114* (21), 7179−7188.
(14) Ozbas, B.; O'Neill, C. D.; Register, R. A.; Aksay, I. A.; Prud'homme, R. K.; Adamson, D. H. *J. Polym. Sci., Part B: Polym. Phys.* **2012**, *50* (13), 910−916.
(15) Hernandez, M.; del Mar Bernal, M.; Verdejo, R.; Ezquerra, T. A.; Lopez-Manchado, M. A. *Compos. Sci. Technol.* **2012**, *73*, 40−46.
(16) Hernández, M.; López-Manchado, M. A.; Sanz, A.; Nogales, A.; Ezquerra, T. A. *Macromolecules* **2011**, *44* (16), 6574−6580.
(17) Boese, D.; Kremer, F. *Macromolecules* **1990**, *23* (3), 829−835.
(18) Havriliak., S.; Negami, S. *Polymer* **1967**, *8* (4), 161−210.
(19) Kremer, F.; Schönhals, A. *Broadband Dielectric Spectroscopy*; Springer: New York, 2003; p 721.
(20) Böttcher, C. J. F.; Bordewijk, P. *Theory of Electric Polarization*; Elsevier: Amsterdam, 1978; Vol. *II*.
(21) Richert, R.; Angell, C. A. *J. Chem. Phys.* **1998**, *108* (21), 9016−9026.
(22) Rueda, D. R.; Garcia-Gutierrez, M. C.; Nogales, A.; Capitan, M. J.; Ezquerra, T. A.; Labrador, A.; Fraga, E.; Beltran, D.; Juanhuix, J.; Herranz, J. F.; Bordas, J. *Rev. Sci. Instrum.* **2006**, *77* (3), 5.
(23) Toki, S.; Sics, I.; Ran, S. F.; Liu, L. Z.; Hsiao, B. S.; Murakami, S.; Senoo, K.; Kohjiya, S. *Macromolecules* **2002**, *35* (17), 6578−6584.
(24) Toki, S.; Sics, I.; Ran, S. F.; Liu, L. Z.; Hsiao, B. S. *Polymer* **2003**, *44* (19), 6003−6011.
(25) Toki, S.; Sics, I.; Hsiao, B. S.; Tosaka, M.; Poompradub, S.; Ikeda, Y.; Kohjiya, S. *Macromolecules* **2005**, *38* (16), 7064−7073.
(26) Tosaka, M.; Murakami, S.; Poompradub, S.; Kohjiya, S.; Ikeda, Y.; Toki, S.; Sics, I.; Hsiao, B. S. *Macromolecules* **2004**, *37* (9), 3299−3309.
(27) Valladares, D.; Yalcin, B.; Cakmak, M. *Macromolecules* **2005**, *38* (22), 9229−9242.
(28) Tosaka, M.; Kohjiya, S.; Murakami, S.; Poompradub, S.; Ikeda, Y.; Toki, S.; Sics, I.; Hsiao, B. S. *Rubber Chem. Technol.* **2004**, *77* (4), 711−723.
(29) Adachi, K.; Kotaka, T. *Prog. Polym. Sci.* **1993**, *18* (3), 585−622.
(30) Tanaka, Y. *Rubber Chem. Technol.* **2001**, *74* (3), 355−375.
(31) Hernández, M.; Carretero-Gonzalez, J.; Verdejo, R.; Ezquerra, T. A.; López-Manchado, M. A. *Macromolecules* **2010**, *43* (2), 643−651.
(32) Gent, A. N. *J. Polym. Sci.* **1955**, *18* (89), 321−334.
(33) Ezquerra, T. A.; Majszczyk, J.; Baltacalleja, F. J.; Lopezcabarcos, E.; Gardner, K. H.; Hsiao, B. S. *Phys. Rev. B* **1994**, *50* (9), 6023−6031.
(34) Sanz, A.; Nogales, A.; Ezquerra, T. A.; Lotti, N.; Munari, A.; Funari, S. S. *Polymer* **2006**, *47* (4), 1281−1290.
(35) Schonhals, A.; Schlosser, E. *Colloid Polym. Sci.* **1989**, *267* (2), 125−132.
(36) Sanz, A.; Nogales, A.; Ezquerra, T. A.; Soccio, M.; Munari, A.; Lotti, N. *Macromolecules* **2010**, *43* (2), 671−679.
(37) Nogales, A.; Ezquerra, T. A.; Denchev, Z.; Sics, I.; Calleja, F. J. B.; Hsiao, B. S. *J. Chem. Phys.* **2001**, *115* (8), 3804−3813.
(38) Kramarenko, V. Y.; Ezquerra, T. A.; Sics, I.; Balta-Calleja, F. J.; Privalko, V. P. *J. Chem. Phys.* **2000**, *113* (1), 447−452.